PRODUCT DESIGN EVALUATION:

STAND MIXER

by

MOHAMMED SAEED ALMHEIRI

YUEKAI KEVIN LU

RAFAE JIBRAEEL SHAFI

Project 2

Mechanical Engineering 41 - Engineering Design II

Tufts University

Medford, Massachusetts

December 15, 2025

TABLE OF CONTENTS

LIST OF DEFINITIONS

Torque	A measure of the tendency of a force to cause rotation about an axis. Units in this paper are newton-meters.
Factor of Safety	The ratio of an allowable stress or load to the actual stress or load used in design. Values greater than one mean the part has a margin.
Duty Cycle	A description of how often and how long the mixer is used over its life, for example, hours per week and years of service.
Design Life	The intended number of cycles or hours that the mixer should operate without failure under the specified duty cycle.
Bearing Life L10	The calculated life at which ten percent of a group of identical bearings are expected to fail under a given load and speed.

LIST OF ABBREVIATIONS, ACRONYMS, AND INITIALISMS

CAD	Computer Aided Design
FBD	Free Body Diagram
FEA	Finite Element Analysis
FoS	Factor of Safety
RPM	Revolutions Per Minute
L10	Bearing life with 10 percent probability of failure
SKF	Svenska Kullagerfabriken
NSK	Nippin Seiko
FAG	Fischer's Automatische Gussstahlkugelfabrik

LIST OF FIGURES AND TABLES

INTRODUCTION

Electric kitchen appliances squeeze a lot of classic machine elements into small, affordable products. Motors, gears, bearings, belts, springs, and linkages all have to work together to deliver useful performance for a long time while still feeling simple and safe for the user. In this project, we treat a consumer stand mixer as a case study and use it to apply the analysis tools from ME41 Engineering Design II to a real product instead of an ideal textbook example.

We focus on the Kitchen in the Box stand mixer [2] used in the ME41 product design evaluation project. The mixer converts electrical power from a single-phase outlet into controlled rotational motion at the paddle attachment in order to mix batters and doughs. After an external inspection, we performed a careful teardown and documented the internal architecture. This revealed three machine element groups that are central to how the mixer works: a compact spur and planetary gear train, a set of rolling element bearings in a plastic housing, and a tilt head hinge and latch mechanism with an internal safety switch.

Each of these subsystems plays a different role. The gear train sets the relationship between motor speed and paddle torque and largely decides whether the mixer can handle thicker doughs. The bearing subsystem carries the radial and thrust loads from the belt and gears and controls how smoothly the shafts run over the life of the product. The hinge subsystem allows the user to tilt the head for access to the bowl, locks it for mixing, and triggers a power cut off when the head is raised so the mixer cannot run in the up position.

The goal of this paper is to evaluate how well these three subsystems support the overall function of the mixer. For each one, we describe the geometry and operating principle, state the assumptions we use for loads and duty cycle, and then apply analytical calculations and, where appropriate, finite element analysis based on methods from Shigley's *Mechanical Engineering Design* [1]. We finish by discussing likely failure modes, design margins, and potential improvements, and then reflect on the overall quality and expected performance of the mixer as a complete product.

GEAR TRAIN SUBSYSTEM

This subsystem is a compact and powerful gear train that delivers a respectable mixing torque, allowing ease and efficiency of use for consumers. Since the motor has no online data providing its maximum RPM or torque, we had to work backwards to determine its values.

Methods

1. A calculation of the gear ratio and speed reduction to optimize output torque
2. Free body diagram
3. SolidWorks CAD model and FEA analysis

The gear train itself operates as follows. The motor pinion drives a belt that interacts with spur gear 1. Spur gear 1 is connected to spur gear 2 co-linearly through a rigid shaft. Spur gear 2 meshes with spur gear 3, which also acts like the sun for the planetary system via a rigid shaft connection through the center bore. The shaft output is fixed to the planet gear, thus spur gear 3 RPM = planet orbit RPM. The planet gear meshes with the fixed ring gear. The mixing paddle is connected to the planet gear via a pin connection that resists free range rotational and translational motion, forcing the paddle to rotate with the planet gear, as well as revolve around the sun.

Labeled and Illustrated Subsystem

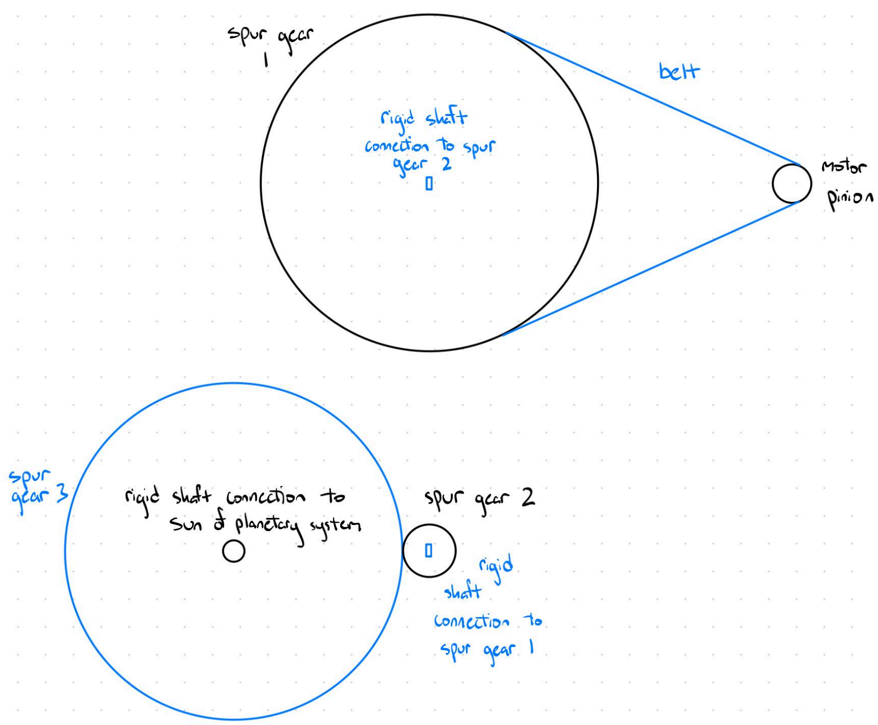

Figure G1: Top-down view of spur gear train with labels showing meshing and connections between gears.

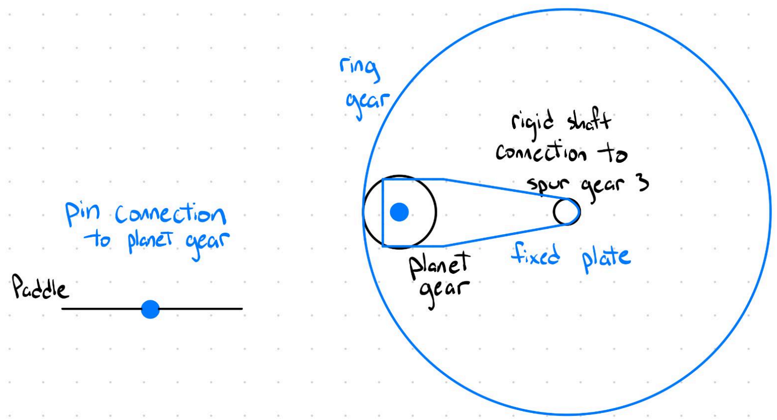

Figure G2: Top-down view of planetary gear system with labels showing connection to spur gear train and into the mixer paddle.

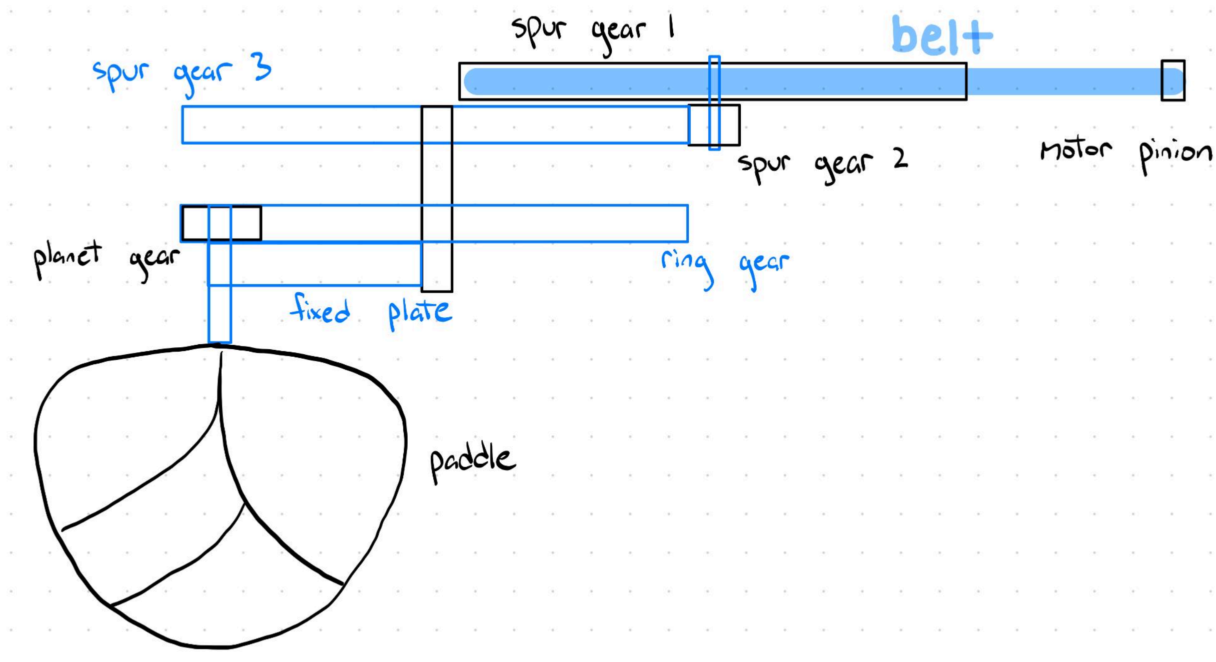

Figure G3: Side view of entire gear train subsystem showing meshing points

Gear Ratio Calculation

The paddle revolved around the bowl 27.5 revolutions every 10 seconds or 165 RPM. This was determined via real-time video. Once this was verified, we counted all the teeth on the gear train, giving us the following table.

Gear	Material	Number of Teeth
Motor Pinion	Steel	13
Belt	Rubber	128
Spur Gear 1	Nylon	95
Spur Gear 2	Steel	9
Spur Gear 3	Nylon	75
Ring Gear	Nylon	41
Planet Gear	Nylon	13

Table G1: Tabulated data of each gear within the gear train subsystem used in analysis. [3] [4]

The train value equation is used to relate output and input speeds and torques.

$$n_L = e n_f \tag{1}$$

The train value can be calculated as follows.

$$e = \frac{product\ of\ driving\ tooth\ numbers}{product\ of\ driven\ tooth\ numbers}$$
$$e = \frac{13 \times 9}{95 \times 75}$$
$$e = 0.016421 \tag{2}$$

Note: Only gears Motor Pinion, Spur Gear 1, Spur Gear 2, and Spur Gear 3 contribute to the paddle revolution about the bowl. Gears Ring Gear and Planet Gear allow for paddle rotation about their own axes.

Using equation (1) and the train value, the motor output can be calculated as follows.

$$n_f = \frac{n_L}{e}$$
$$n_f = \frac{165\ RPM}{0.016421}$$
$$n_f = 10,048.1\ RPM$$

Torque Calculation

We can determine the no-load torque from the maximum rpm. The motor housing indicates 300W; therefore, we can determine the no-load torque using the following formula.

$$T = \frac{P}{\omega}$$
$$\omega = \frac{2\pi \times RPM}{60}$$
$$T = \frac{P \times 60}{2\pi \times RPM}$$
$$T = \frac{300 \times 60}{2\pi \times 10000}$$
$$T = 0.286\ Nm$$

This relationship is the relative spin of a planet gear per revolution around a sun, when the ring gear is fixed.

$$Planet\ spin\ per\ revolution = \frac{N_R}{N_p} - 1$$
$$Planet\ spin\ per\ revolution = \frac{41}{13} - 1$$
$$Planet\ spin\ per\ revolution = 2.15 \qquad (3)$$

The following is the total gear ratio and speed reduction from the spur gears and planetary gear system.

$$GR = \frac{1}{e} \times \frac{1}{Planet\ spin\ per\ revolution}$$
$$GR = \frac{1}{0.016421} \times \frac{1}{2.15}$$
$$GR = 28.32:1$$

We can use the same train value (2) alongside the planet spin per revolution to determine paddle output speed and output torque.

$$RPM_{output} = RPM_{about\ bowl}\,(2.15)$$
$$RPM_{output} = 165RPM\,(2.15)$$
$$RPM_{output} = 354.75\ RPM$$

$$T_{output} = T(e)(\frac{1}{2.15})$$
$$T_{output} = 0.286\ Nm\,(0.016421)(\frac{1}{2.15})$$
$$T_{output} = 8.10\ Nm$$

This image shows the paddle attachment where the maximum edge distance from the center of rotation is r = 5.3 cm.

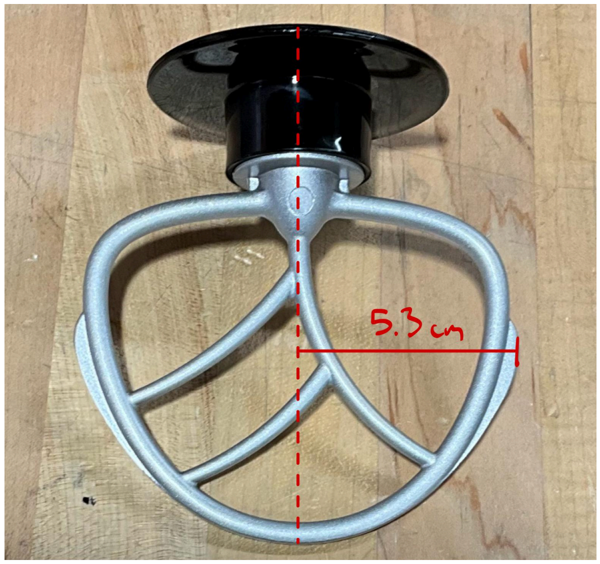

Figure G4: Paddle attachment showing measurements for analysis

The force at the edge of the paddle can be calculated from this torque using the following formula.

$$F_{paddle} = \frac{T_{output}}{r}$$

$$F_{paddle} = \frac{8.10\ Nm}{0.053\ m}$$

$$F_{paddle} = 152.83\ N$$

Free Body Diagrams and Force and Torque Propagation

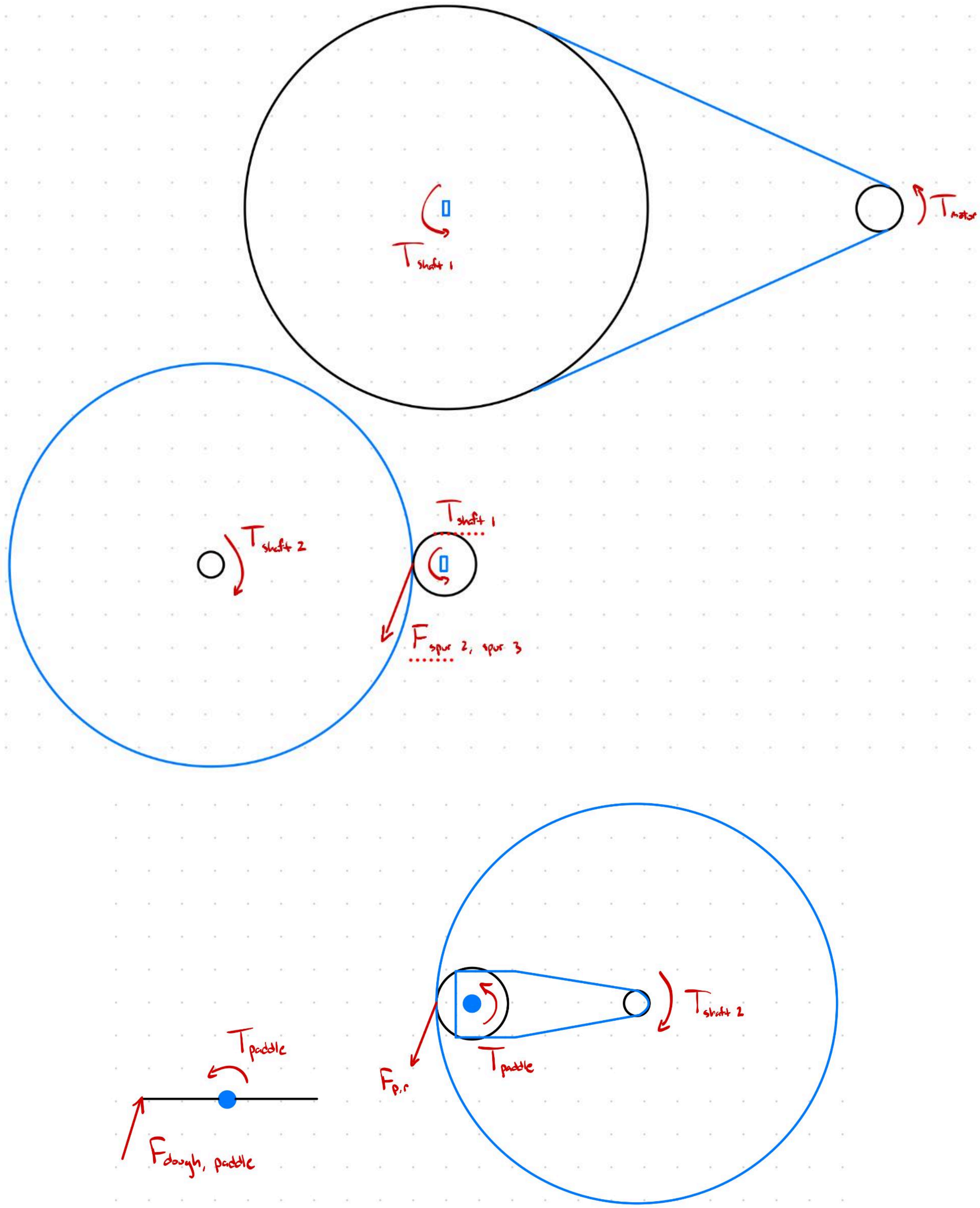

Figure G5: Free body diagram showing force and torque propagation throughout the gears to the paddle attachment

SolidWorks CAD

The SolidWorks CAD model and FEA analysis were an interesting challenge. The CAD model was created on Onshape, with the help of the spur gear custom feature. I assumed a pressure angle of 20° for both gears with a module of 0.125 cm. I also added a root filet of ⅓ and a backlash of 0.02 cm on both gears to allow for smoother meshing in the SolidWorks motion simulation. I exported these parts as SolidWorks files and created the assembly below.

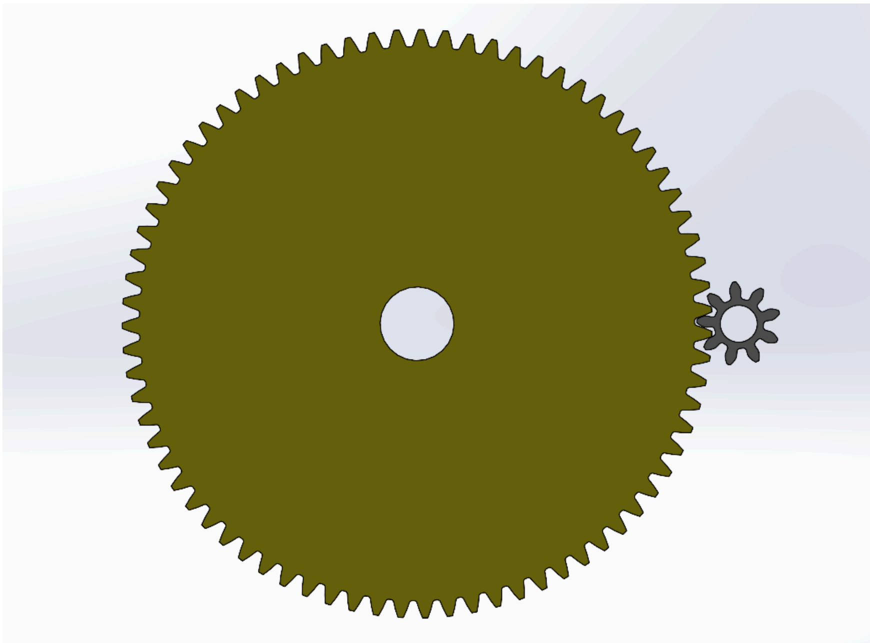

Figure G6: SolidWorks CAD gear model with a larger, yellow nylon spur gear meshing with a smaller steel spur gear

SolidWorks Motion Study

After the proper mates were applied, the motion study yielded this cool gif. The small steel gear is spinning at 20 RPM clockwise, spinning the larger nylon gear 2.4 RPM counterclockwise from the 8.33:1 gear ratio provided.

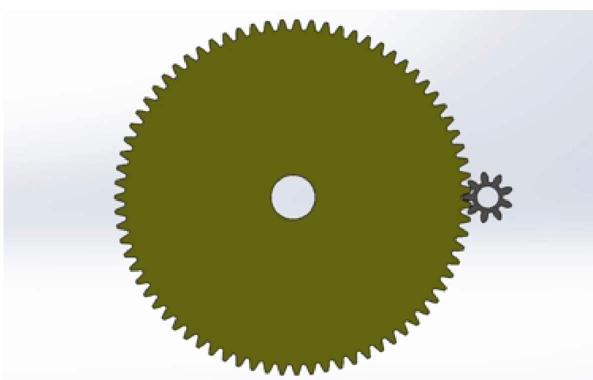

Figure G7: GIF of the SolidWorks motion study

SolidWorks FEA

To set up the static study FEA, material, fixtures, connections, torque, and mesh had to be applied. After doing some research, it was found that Nylon (PA6) and 8620 steel were commonly used for their high fatigue strength, rigidity, and heat resistance. Out of the two materials, SolidWorks only had PA6. The material chosen in its place is AISI 4130 steel. This material also has good fatigue strength and toughness. For the fixtures, the spur gear 2 drives the larger spur gear 3; therefore, spur gear 3 was fixed, and spur gear 2 was a hinge. The connections also had to be adjusted to prevent penetration between the gears. Finally, a torque of 2.09 Nm was applied to the smaller spur gear 2 using calculations from the first gear ratio and motor output torque, and then the geometries were meshed using control meshes around the contact surfaces.

Below are images of the FEA setup and results:

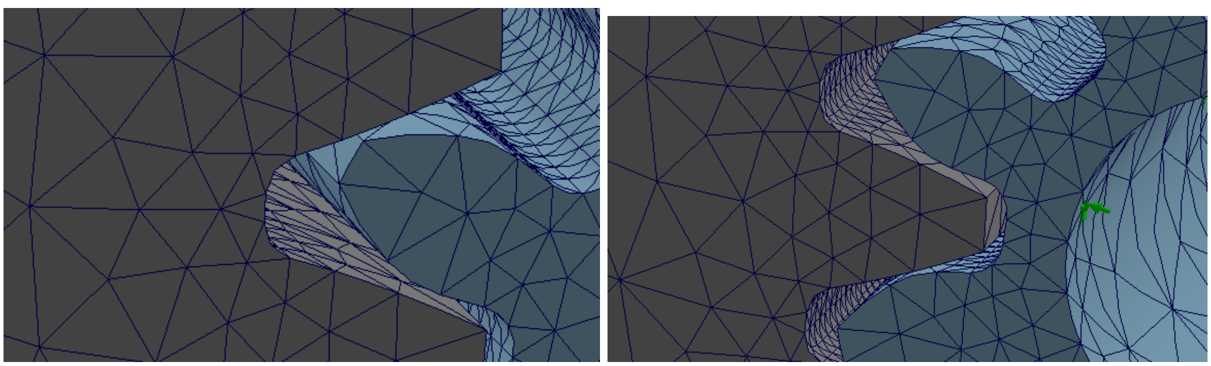

Figure G8: Detailed mesh control used by SolidWorks FEA solver

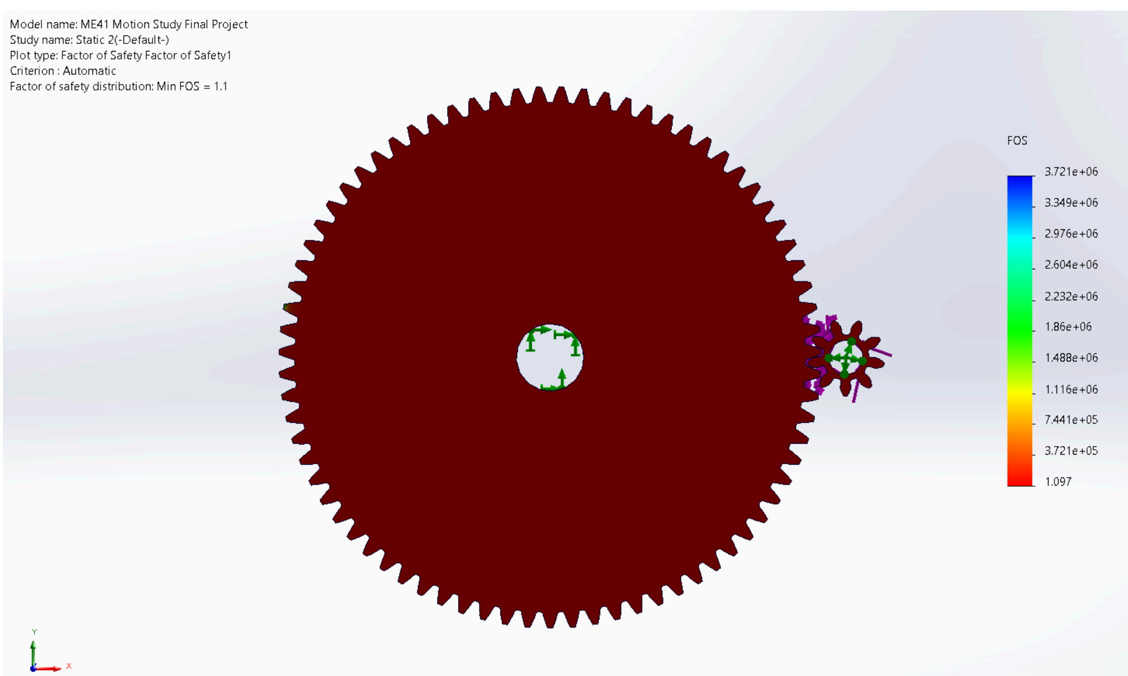

Figure G9: SolidWorks FEA FoS heat map

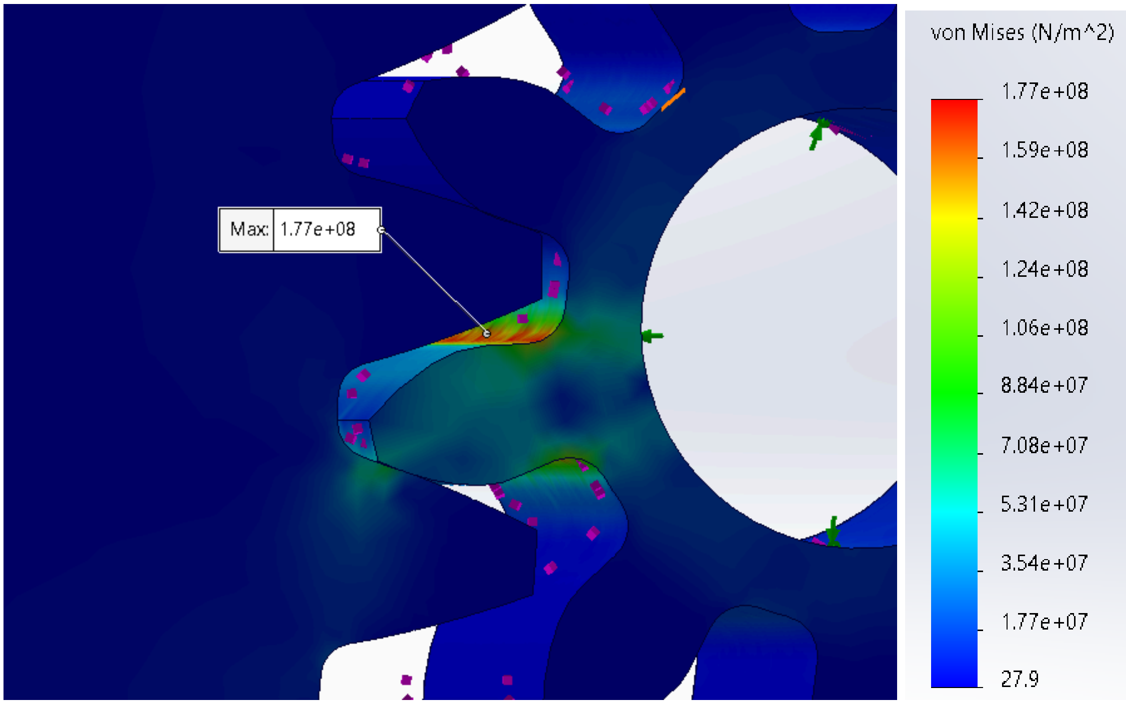

Figure G10: SolidWorks FEA results showing stresses at gear meshing

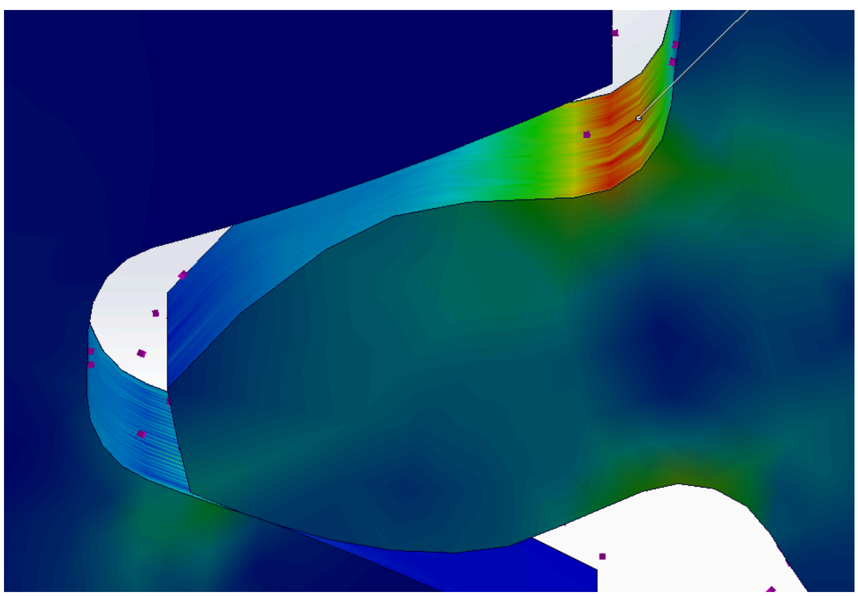

Figure G11: SolidWorks FEA results showing stresses at gear meshing continued

The gear train analysis yielded many interesting results. The stresses show very reasonable maximum values for steel gears, while the nylon gears experience significantly less stress. The gear system also has a factor of safety, slightly above 1, meaning that variation in stresses is risky, especially when it comes to materials like nylon. However, this gear train is quite robust when it comes to its speed reduction and torque amplification.

BEARING SUBSYSTEM

The bearing used in the stand mixer is a steel deep-groove ball bearing positioned in a plastic gearbox housing. It helps support the shaft that carries a belt pulley on one end and transmits power to the internal geartrain. From observation, the bearings primary function is to:

- Radially support the shaft and help maintain alignment between the belt pulley and the downstream gear train elements
- React against constant radial loads primarily coming from the belt torsion
- React against secondary radial loads from the gear forces
- Help support against small axial loads that may arise from gear misalignment

Load Path

Initially, the motor torque is transmitted through a belt drive to a pulley mounted on an intermediate shaft. The belt thereby constantly applies an inward radial force on the pulley. The shaft then transmits torque to the geartrain. This is where we get the introduction of gear meshes, adding in radial separating forces and small axial forces. Finally, forces from the ball bearing are transferred to its housing, which is transferred to the general mixer structure.

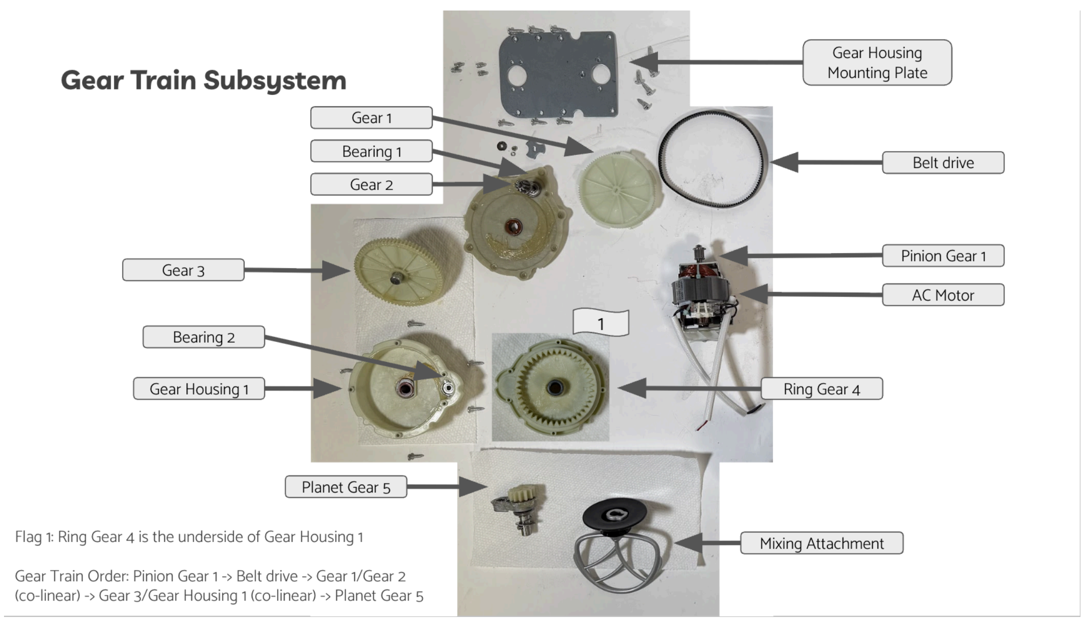

Figure B1: Disassembled gear train subsystem highlighting the bearings positioning in within the subsystem

<u>Bearing Identification and Measurements:</u>

Upon researching and inspection of the bearings, the most reasonable bearing is the 608 bearing (8x22x7 mm). It is widely used in appliances and gearboxes. Its load capacity also suits our load analysis of small radial and minor thrust loads. This isn't a perfect assumption, but later on in our calculations, we will take this into account by taking note of upper and lower bounds.

Parameter	Symbol	Value
Bore (ID)	d	8 mm
Outer diameter	D	22 mm
Width	B	7 mm
Bearing type	—	Deep-groove ball bearing
Seal/shield	—	Open (no seals)

Table B1: 608 Bearing Geometry

Bearing catalog values:
Suitable for ABMA/ISO life calculations

Property	Symbol	Typical value
Dynamic load rating	C	**3.3 kN**
Static load rating	C_0	**1.37 kN**
Limiting speed (greased)	—	30,000 rpm
Ball count	—	6 balls
Contact angle	—	0° (radial bearing)

Table B2: Bearing catalog values (Suitable for ABMA/ISO life calculations)

Housing, Mounting, and Bearing Seat Geometry

The plastic used is definitely from injection molding, which leads me to believe it is glass-filled nylon or potentially acetal.

Feature	Observation
Fit type	Light press fit
Retention	Housing clamping, no snap ring
Ribs	Radial stiffening ribs
Axial constraint	Bearing clamped between housing halves
Lubrication	Grease in housing cavity

Table B3: Initial observations of bearing placement and its environment

From measuring with a micrometer, I got the following values for the system geometry:

Parameter	Symbol	Value
Shaft diameter at bearing	d_s	8 mm
Bearing → pulley centerline	L_p	25 mm
Bearing → gear mesh	L_g	12.5 mm
Bearing span (to next support)	L_{span}	50 mm

Table B4: Bearing measurements

<u>Mixer Operations into Bearing Loads</u>

From our work on the gearing subsystem, we have calculated a lot of the necessary variables needed to start solving for our shaft speed and torque on the bearing.

The torque that acts on the shaft supported by the bearing itself is important to take into account. To solve for it, we can account for the overall speed reduction due to the gear train upstream of the bearing. Because the torque scales inversely with the speed, we can solve the shaft torque by dividing the motor torque by the train value. This is assuming an ideal power transmission.

$$T_{shaft} = \frac{T_{motor}}{e}$$

$$T_{shaft} = \frac{0.286}{0.016421} = 17.4\ Nm$$

The torque is then transmitted along the shaft before being converted into a tangential force at the belt pulley.

$$F_t = \frac{T_{shaft}}{r_p} = \frac{17.4}{0.015} = 1160\ N$$

In the belt drive system, we need to account for the difference in tension between the tight and slack sides of the belt. This is what creates the torsion transmission. The tangential force must therefore be equal to the difference between the two belt tensions. Due to the impracticality of measuring belt tensions for our stand mixer, we can assume that a ratio of our tension differences is a fair assumption for the value of R. This is typical of many belt drives in small appliances. We can then plug into our total radial load formula to yield our resultant belt radial load to be 2320N.

$$F_t = T_1 - T_2$$

$$\frac{T_1}{T_2} = R$$

$$F_{belt} \approx T_1 + T_2$$

$$F_{belt} = \frac{R+1}{R-1} F_t$$

$$F_{belt} = 2F_t = 2320\ N$$

The tangential force, which is transmitted through the spur gear mesh, represents the load responsible for the torque transfer from the gear teeth. It also adds radial loading to the bearing from shaft reactions.

$$F_{t,g} = \frac{T_{shaft}}{r_g}$$

$$F_{t,g} = \frac{17.4}{0.025} = 696\ N$$

The tangential gear force creates a radial separating force from the pressure angle of the spur gears. This force acts perpendicular to the direction of motion. Common spur gear designs in small appliances tend to have a pressure angle of around, 20° so we will assume that for this analysis.

$$F_{r,g} = F_{t,g} tan\phi$$

$$F_{r,g} = 696 \times 0.364 = 253\, N$$

The total bearing load that acts on the bearing, we assume to be acting in the same direction, resulting in a pretty conservative estimate of the bearing radial load.

$$F_R = F_{belt} + F_{r,g}$$

$$F_R = 2320 + 253 = 2570\, N$$

Lastly, to account for adverse effects from potential manufacturing errors, potential misalignment, or assembly imperfections, we will assume that the spur gear generates a small amount of axial force on the bearing.

$$F_A = 0.1F_R$$

$$F_A = 257\, N$$

<u>Dynamic Bearing Load (ABMA)</u>

To effectively analyze the true forces that go through a rolling element bearing, we will use the ABMA bearing life methodology [5]. We will replace the combined radial and axial loads with a single equivalent dynamic load, P.

For a deep groove ball bearing, the equivalent dynamic load equation is:

$$P = XF_r + YF_a$$

Where:

- F_R is the resultant radial load on the bearing
- F_a is the axial load
- X and Y are load factors dependent on the bearing type and the ratio of $\frac{F_a}{F_r}$

The ratio of axial force to radial force determines the relative importance of axial loading. We can calculate this by dividing $\frac{F_a}{F_r}$.

$$\frac{F_a}{F_r} = \frac{257}{2570} = 0.10$$

The ABMA guidance indicators suggest that we should consider that radial loading is far more dominant than bearing fatigue behaviour for deep-groove ball bearings. *(SKF Group)*. When the axial-to-radial load ratio is less than 0.3, radial load is taken as unity, while a conservative value for axial load is applied. Therefore,

$$X = 1.0\,,\; Y = 0.56$$

We can substitute our found values into the equivalent load equation:

$$P = (1.0)(2570) + (0.56)(257) = 2714N$$

This load incorporates both the dominant belt-induced radial force and the conservative estimate of axial loading that may be caused by manufacturing errors or misalignment.

Bearing Life Analysis

After inferring that the bearing is indeed a standard 608 deep-groove ball bearing, we confirmed with several manufacturing catalogs (SKF, NSK, FAG) that the typical dynamic load value is approximately $3.3\ kN$.

$$C = 3300N$$

To solve for our bearing life, we will use the following equation for L_{10} which represents the number of revolutions that 90% of the same bearings are expected to exceed before showing their first signs of fatigue. For ball bearings, the life exponent is 3.

$$L_{10} = \left(\frac{C}{P}\right)^p \times 10^6$$

Substituting our known values into the equation:

$$L_{10} = \left(\frac{3300}{2714}\right)^3 \times 10^6 = 1.80 \times 10^6\ revolutions$$

To calculate the bearing life in hours, we divide by the rotational speed of the shaft. As we found in the gear analysis, our RPM is 165.

$$L_{10}(h) = \frac{1.80\times10^{6}}{60 \times 165} = 182\ hours$$

However, since we were unable to identify directly from the manufacturer of the stand mixer what the exact bearing is, we will take upper and lower bounds to take into account sensitivity, to give a plausible range of the number of hours. We will alter the dynamic load value by 300N in both ways.

Upper Bound:

$$C = 3600N$$

$$L_{10} = (\frac{3600}{2714})^{3}\times 10^{6} = 2.32\times10^{6}\ revolutions$$

$$L_{10}(h) = \frac{2.32\times10^{6}}{60 \times 165} = 234\ hours$$

Lower Bound:

$$C = 3000N$$

$$L_{10} = (\frac{3000}{2714})^{3}\times 10^{6} = 1.35\times10^{6}\ revolutions$$

$$L_{10}(h) = \frac{1.35\times10^{6}}{60 \times 165} = 136\ hours$$

Therefore, our predicted bearing rating life ranges from around 136 hours to 234 hours, depending on the assumed dynamic load rating. However, from our inference and research into the bearing's dynamic load rating, we predict a more exact value of 182 hours. This is a relatively short fatigue life, which is driven by the large constant radial load imposed by the belt tension. This number may be further reduced due to real-world service life, misalignment, lubrication degradation, housing compliance, and general manufacturing errors.

<u>Plastic Housing Effects and Real-World Life Reduction</u>

The bearing life we calculated assumes ideal operating conditions. These things like perfect alignment, rigid housing, and steady loading. Within the plastic housing, there are several real-world factors that affect the effective service life relative to the theoretical rating life.

Housing compliance and misalignment:

Plastic housing, compared to metallic housing, has a significantly lower stiffness. Under the constant load, it can lead to elastic deformation of the plastic housing. This can lead to angular misalignment of the bearing races. Over time, this misalignment can increase local contact stresses and accelerate fatigue.

Press-fit relaxation and creep:

A general trend with plastic materials is that they are prone to creep under sustained load. Over time, the interference between the bearing outer race and the housing decreases, allowing more movement of the bearing. This can assist in misalignment due to vibrations through the bearing, which contributes to a reduced bearing life.

Contamination, lubrication, and temperature:

The bearing operates within a sealed gearbox with a large amount of grease as lubrication. This can may wear away after repeated use, especially if not stored properly in the right environment. Poorly stored grease could attract dust and moisture. Elevated operating temperatures can further decrease the grease's effectiveness. This all leads to an increase in friction and wear on the bearing.

Cyclic loading and duty cycle:

The bearing operates at a modest rotational speed, but it still experiences a high amount of load cycles due to the product's nature as a start/stop mechanism. These cyclic conditions induce stress variations beyond the steady loading we assumed in the analysis, which all accelerate fatigue.

Summary of Bearing Analysis

The results of the analysis show that its primary role is to maintain radial support and prevent any shaft misalignment under large continuous loads. The calculated equivalent dynamic load showcases that the radial loading is the primary factor in causing fatigue damage, whilst axial loading is also a contributing factor. The predicted rating life also suggests that the rolling-contact fatigue is unlikely to be the only factor leading to limiting the life of the bearing. We went into depth about how some other real-world effects can also contribute to this.

Overall, the results indicate that the bearing fulfills its job as a low-cost radially loaded support element. However, its performance in the long term is governed partly by external factors, in other elements of the stand mixer's structure and usage.

HINGE SUBSYSTEM

The hinge subsystem allows the stand mixer head to tilt up for loading ingredients and then lock down during operation. It includes the plastic head and base housings, a steel hinge pin with a torsion spring, a steel travel rod with a compression spring and push button, and two stamped steel latch plates. Together, these parts convert a small user push on the front button into rotation of the head and then hold the head securely in either the up or down position. In addition to supporting the head, the hinge mechanism actuates an internal safety switch so that the motor power is cut whenever the head is in the raised position. This prevents the mixer from running with the head up.

When the button is not pressed, the compression spring pushes the travel rod forward. In this state, the thicker sections of the rod rest against the ends of curved slots in the latch plates, which prevents rotation and locks the head. When the user presses the button, the rod slides backward until its thin central section aligns with the slots. The head can then rotate between the up and down positions while the rod follows the curved path of the slots. Releasing the button allows the spring to push the rod forward again so the thick sections re-engage the slots and lock the head at the new position.

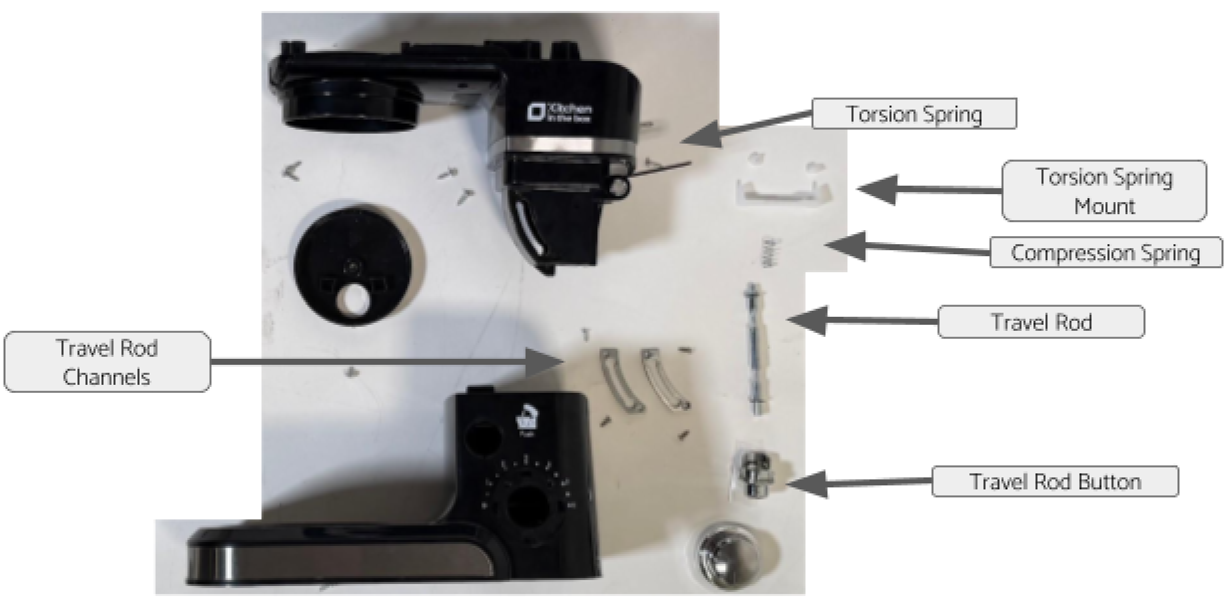

Figure H1: Disassembled hinge subsystem of the stand mixer showing the torsion spring, travel rod, compression spring, latch plates, and push button.

Methods and Assumptions

The hinge analysis used the following tools:

1. A free body diagram of the mixer head cut free from the base to obtain moments about the hinge.

2. Torsion spring relations and material properties from Shigley's Mechanical Engineering Design [1] to estimate spring torque and wire stress.

3. Axial stress and contact pressure calculations for the travel rod and latch plates.

4. Load cases based on head weight and realistic user pushes on the head.

The head is modeled as a rigid body. The mass of the tilting head, which includes the motor, gear train, and upper housing, was estimated from the total product mass and measured component masses as

$$m_{head} \approx 2.0\ kg$$

where m_{head} is the mass of the tilting assembly.

Distances from the hinge axis along the head are

$$d_{cg} = 0.20\ m$$

$$L_{lat} = 0.10\ m$$

$$L_{user} = 0.15\ m$$

Here, d_{cg} is the horizontal distance from the hinge to the approximate head center of mass, L_{lat} is the distance from the hinge to the latch contact point on the travel rod, and L_{user} is the distance from the hinge to a natural user push location on the top of the head.

A conservative user push is taken as

$$F_{user} = 50\ N$$

where F_{user} is the vertical downward force from a strong hand push.

The torsion spring around the hinge pin has the measured geometry

$$d_w = 2.2\,mm$$
$$D = 12\,mm$$
$$N_a = 8$$
$$\theta = 60°$$

where d_w is the wire diameter, D is the mean coil diameter to the wire centerline, N_a is the number of active coils, and θ is the head rotation between the fully up and down positions.

The latch plates are cut from sheet steel with a thickness

$$t_{plate} \approx 0.89\,mm$$

and slot width at the contact location

$$w_{slot} \approx 5.8\,mm$$

The thin section of the travel rod has a diameter

$$d_r = 4.5\,mm$$

which is used to evaluate axial stress in the rod.

Symbol	Description	Value	Unit	Note
m_{head}	Estimated mass of tilting head	2.0	kg	Total mixer mass minus base, bowl, attachments, splash cover
d_{cg}	Distance from hinge to head center of mass	0.20	m	Measured along head arm
L_{lat}	Distance from hinge to latch contact	0.10	m	Hinge axis to travel rod contact in latch plates
L_{user}	Distance from hinge to user push point	0.15	m	Approximate location where user pushes on head
F_{user}	Assumed user push on the head	50	N	Strong one hand push
g	Gravitational acceleration	9.81	m/s^2	Standard value

d_w	Torsion spring wire diameter	2.2	mm	Measured with calipers
D	Torsion spring mean coil diameter	12	mm	Outer diameter minus one wire diameter
N_a	Number of active torsion coils	8	-	Coils that twist under load
θ	Head rotation between up and down	60	deg	Measured with a protractor
E	Elastic modulus of spring steel	210	GPa	From Shigley's material tables
t_{plate}	Latch plate thickness	0.89	mm	Measured with calipers
w_{slot}	Latch slot width at rod contact	5.8	mm	Measured with calipers
d_r	Travel rod thin diameter	4.5	mm	Measured with calipers
L_{free}	Compression spring free length	20.5	mm	Measured off the mixer
d_c	Compression spring wire diameter	0.88	mm	Measured with calipers
D_c	Compression spring mean coil diameter	6.4	mm	Outer diameter minus one wire diameter
F_{spring}	Assumed preload from compression spring	30	N	Representative value inside estimated range 20 to 40 N

Table H1: Hinge subsystem measurements and modeling assumptions used in the analysis.

FBD and Global Moment

Figure H2 shows the mixer head cut free from the base. The loads acting on the head are

- head weight $W_{head} = m_{head}g$ acting downward at a distance d_{cg}
- user pushes F_{user} acting downward at a distance L_{user}
- latch force F_{lat} acting upward at a distance L_{lat}
- torsion spring torque T_{spring} applied at the hinge in the counterclockwise direction

Here $g = 9.81 m/s^2$ is the gravitational acceleration, and F_{lat} is the reaction transmitted through the travel rod into the latch plates.

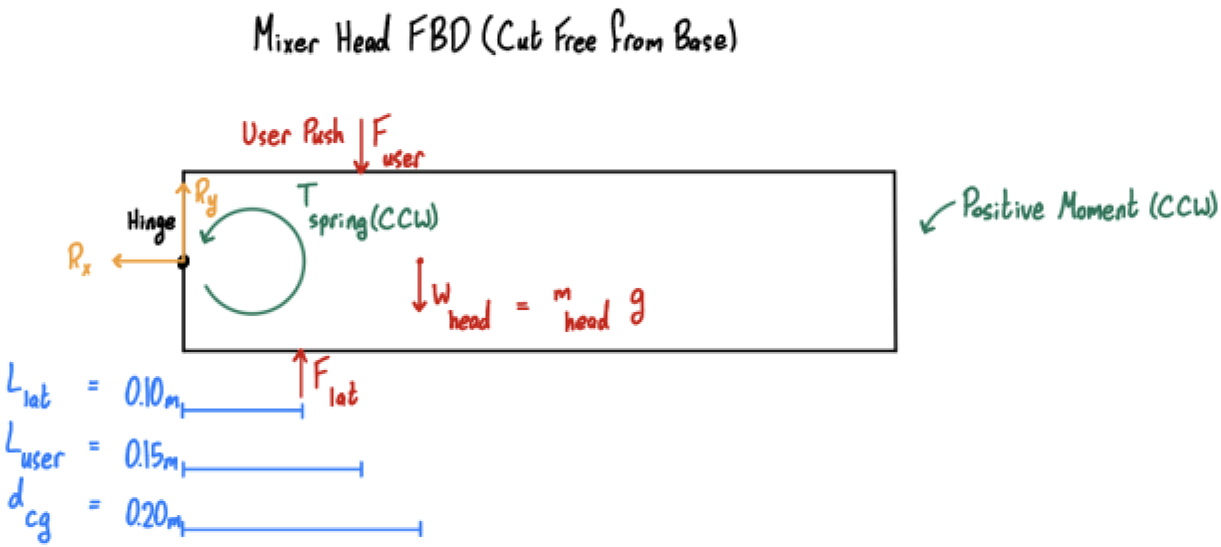

Figure H2: Free body diagram of the mixer head cut free from the base, indicating the head weight, latch force, user push, torsion spring torque, and the distances from the hinge to each of these forces.

The moment about the hinge due to head weight is

$$M_W = m_{head} g d_{cg}$$
$$M_W = (2.0\ kg)(9.81\ m/s^2)(0.20\ m)$$
$$M_W = 3.9\ Nm \tag{1}$$

where M_W is the gravitational moment.

The moment from the user push is

$$M_{user} = F_{user} L_{user}$$
$$M_{user} = (50\ N)(0.15\ m)$$
$$M_{user} = 7.5\ Nm \tag{2}$$

The total design moment that the hinge must resist in the locked position is

$$M_{total} = M_W + M_{user}$$
$$M_{total} = 3.9\ Nm + 7.5\ Nm$$
$$M_{total} = 11.4\ Nm \tag{3}$$

where M_{total} is the combined moment from head weight and user push.

Torsion Spring Torque and Safety Factor

The torsion spring provides a restoring torque that offsets part of the head weight and gives the head a light feel during lifting. Using relations for round wire helical springs from Shigley [1], the torsion rate for one full revolution of twist is

$$R_{360} = \frac{Ed_w^4}{10.8DN_a}$$
$$R_{360} = \frac{(210 \times 10^3\ MPa)(2.2^4\ mm^4)}{10.8(12\ mm)(8)}$$
$$R_{360} \approx 4.76\ N\ per\ 360° \tag{4}$$

where R_{360} is the torque required for 360° of twist, $E = 210\ GPa$ and is the elastic modulus of spring steel.

The torsion rate per degree of rotation is

$$k_\theta = \frac{R_{360}}{360}$$
$$k_\theta = \frac{(4.7\ Nm)}{360°}$$
$$k_\theta \approx 0.013\ Nm\ per\ degree \tag{5}$$

For the measured head rotation of

$$\theta \approx 60°$$

the torque in the locked position is

$$T_{spring} = k_\theta \theta$$
$$T_{spring} = (0.013\ Nm\ per\ degree)(60°)$$
$$T_{spring} \approx 0.79\ Nm \tag{6}$$

The corresponding maximum bending stress in the spring wire is estimated with a curvature factor K as

$$\sigma_{spring} = K \frac{32T_{spring}}{\pi d_w^3}$$

$$\sigma_{spring} = (1.2) \frac{32(0.79\ Nm)(10^3\ Nmm\ per\ Nm)}{\pi(2.2^3\ mm^3)}$$

$$\sigma_{spring} \approx 9.1 \times 10^2\ MPa \tag{7}$$

where σ_{spring} is the bending stress in the wire, and $K = 1.2$ accounts for curvature and stress concentration.

For music wire with yield strength

$$\sigma_{yield} \approx 2,050\ MPa$$

the factor of safety against yielding is

$$FoS_{spring} = \frac{\sigma_{yield}}{\sigma_{spring}}$$

$$FoS_{spring} = \frac{2,050\ MPa}{910\ MPa}$$

$$FoS_{spring} \approx 2.3 \tag{8}$$

which indicates a comfortable margin for the torsion spring.

Latch Force and Contact Pressure

The remainder of the head moment is carried by the latch through the travel rod and steel plates. Using the free body diagram in Figure H2, the equilibrium for the head weight only case is

$$M_W = T_{spring} + F_{lat}L_{lat}$$

$$3.9\ Nm = 0.79\ Nm + F_{lat}(0.10\ m)$$

$$F_{lat} \approx 31\ N \tag{9}$$

where F_{lat} is the latch force in the travel rod.

For the strong user push case, the total moment is given by Eq. (3), and the equilibrium becomes

$$M_{total} = T_{spring} + F_{lat,\,misuse}L_{lat}$$

$$11.4\,Nm = 0.79\,Nm + F_{lat,\,misuse}(0.10\,m)$$
$$F_{lat,\,misuse} \approx 1.1 \times 10^{2}\,N \tag{10}$$

where $F_{lat,\,misuse}$ is the latch force under this heavier loading.

Each latch plate has a thickness t_{plate} and a slot width w_{slot}. With one plate on each side of the rod, the total projected contact area is

$$A_{lat,\,total} = 2t_{plate}w_{slot}$$
$$A_{lat,\,total} = 2(0.89\,mm)(5.8\,mm)$$
$$A_{lat,\,total} \approx 10.3\,mm^{2} \tag{11}$$

where $A_{lat,\,total}$ is the combined projected contact area of both latch plates

The average contact pressure during normal use is

$$p_{lat} = \frac{F_{lat}}{A_{lat,\,total}}$$
$$p_{lat} = \frac{31\,N}{10.3\,mm^{2}}$$
$$p_{lat} \approx 3.0\,MPa \tag{12}$$

For the strong user push case, the pressure is

$$p_{lat,\,misuse} = \frac{F_{lat,\,misuse}}{A_{lat,\,total}}$$
$$p_{lat,\,misuse} = \frac{1.1\times10^{2}\,N}{10.3\,mm^{2}}$$
$$p_{lat,\,misuse} \approx 10\,MPa \tag{13}$$

These contact pressures are much lower than typical allowable values for mild steel, so yielding of the latch plates is not expected. Wear at the sliding surfaces is more likely to control life.

<u>Compression Spring and Travel Rod Stress</u>

The compression spring on the travel rod provides preload that keeps the latch engaged when the user is not pressing the button. The measured free length is

$$L_{free} \approx 20.5\,mm$$

with a wire diameter

$$d_c \approx 0.88\, mm$$

and mean coil diameter

$$D_c \approx 6.4\, mm$$

Although the exact spring rate was not measured, the small compression in the latched position suggests a preload in the range

$$F_{spring} \approx 20\ to\ 40\ N$$

For the analysis, a representative value of

$$F_{spring} = 30\ N$$

was used, where F_{spring} is the axial force on the travel rod.

The cross-sectional area of the thin portion of the rod is

$$A_r = \frac{\pi d_r^2}{4}$$
$$A_r = \frac{\pi (4.5\, mm)^2}{4}$$
$$A_r \approx 15.9\, mm^2 \tag{14}$$

The corresponding axial stress in the rod is

$$\sigma_r = \frac{F_{spring}}{A_r}$$
$$\sigma_r = \frac{30\ N}{15.9\, mm^2}$$
$$\sigma_r \approx 1.9\, MPa \tag{15}$$

which is several orders of magnitude below the yield strength of steel. Even if the mixer is opened and closed many thousands of times, fatigue in the rod at this stress level is not expected to be critical.

<u>Summary of Hinge Results</u>

Case	Description	Main Inputs	Key Results	Comment
1	Head weight only	$m_{head} = 2.0\,kg$ $d_{cg} = 0.20\,m$ $L_{lat} = 0.10\,m$	$M_W = 3.9\,Nm$ $F_{lat} \approx 31\,N$ $p_{lat} \approx 3.0\,MPa$	Locked running condition with no extra user push
2	Head weight plus strong user push	Case 1 + $F_{user} = 50\,N$ $L_{user} = 0.15\,m$	$M_{total} = 11.4\,Nm$ $F_{lat,\,misuse} \approx 1.1 \times 10^2\,N$ $p_{lat,\,misuse} \approx 10\,MPa$	Aggressive but realistic user loading on the head
3	Torsion spring sizing	$d_w = 2.2\,mm$ $D = 12\,mm$ $N_a = 8$ $\theta = 60°$ $E = 210\,GPa$	$T_{spring} \approx 0.79\,Nm$ $\sigma_{spring} \approx 9.1 \times 10^2\,MPa$ $FoS_{spring} \approx 2.3$	Uses helical spring relations and music wire properties
4	Travel rod preload	$F_{spring} = 30\,N$ $d_r = 4.5\,mm$	$A_r \approx 15.9\,mm^2$ $\sigma_r \approx 1.9\,MPa$	Axial stress is very small, fatigue is not expected critical

Table H2: Summary of hinge subsystem load cases and the corresponding calculated results.

The hinge subsystem analysis shows that

- The torsion spring provides about $0.79\,Nm$ of torque at full deflection with a factor of safety of about 2.3 in the wire
- The latch plates carry latch forces of about $31\,N$ in normal use and about $1.1 \times 10^2\,N$ in the strong push case, while contact pressures remain between three and ten megapascal
- Axial stresses in the travel rod are about two megapascals, which is negligible compared with the steel strength

These results indicate that strength is not the limiting factor for the hinge subsystem. Long-term issues are more likely to involve wear in the latch slots, gradual loss of torsion spring stiffness, or possible cracking of the surrounding plastic housing if the mixer is dropped. Functionally, the hinge subsystem successfully keeps the mixer head securely locked during mixing while still allowing the user to tilt the head easily with a single button press.

CONCLUSION

The stand mixer we analyzed combines a compact gear train, small ball bearings, and a simple hinge and latch into one consumer product. Studying these three subsystems together shows how the mixer balances torque capability, life, cost, and user safety.

For the gear train, counting teeth and measuring paddle motion gave a total speed reduction of roughly twenty-eight to one and an output torque on the order of eight newton meters. This is enough for typical home mixing tasks, but SolidWorks results for the nylon gears suggest factors of safety only slightly above one in the most highly loaded regions. The mixer can do the job, yet the gears do not have much extra margin for overload or material variation.

The bearing subsystem carries belt and gear loads and quietly sets the useful life of the mixer. Using a representative deep groove ball bearing and estimating the dynamic load led to a catalog life in the range of one hundred thirty to two hundred thirty hours. This is acceptable for an inexpensive appliance that sees occasional use, but high radial loads and a flexible plastic housing will likely reduce real-life performance and may lead to noise or looseness before any gear failures occur.

The hinge subsystem is mainly driven by user interaction. Modeling the head as a rigid body showed that head weight alone produces modest locking loads, while a strong push from a user can generate hinge moments of around eleven newton meters. The torsion spring and steel latch plates carry these loads with comfortable strength margins, and axial stresses in the travel rod are low. The more realistic concerns are wear in the latch slots, gradual loss of spring stiffness, or damage to the plastic housing if the mixer is dropped. The hinge also integrates an internal safety switch so that the motor cannot run when the head is up, which is an important part of the overall design.

Overall, the mixer meets its basic design goals. It delivers adequate torque, runs on reasonably sized bearings, and gives the user easy and safe access to the bowl. At the same time, the analysis points to straightforward improvements such as reducing belt tension, stiffening the bearing support, or increasing the margin in the nylon gears. From an Engineering Design II perspective, this project showed how free-body diagrams, stress calculations, and factors of safety from class can be applied to a real product with incomplete information, and how that analysis can still support clear judgments about design adequacy and possible upgrades.

REFERENCES

[1] J. K. Nisbett, *Shigley's Mechanical Engineering Design*, 11th ed., McGraw-Hill, 2024.

[2] Kitchen in the Box, "Kitchen in the box Stand Mixer, 3.2Qt Small Electric Food Mixer, 6 Speeds Portable Lightweight Kitchen Mixer for Daily Use with Egg Whisk, Dough Hook, Flat Beater," Amazon product page, Amazon, accessed January 2026. Available at: https://www.amazon.com/Kitchen-box-Electric-Portable-Lightweight/dp/B09BVCPSBT

[3] Shenzhen Quanda Plastics Co., Ltd., "How To Choose Materials For Engineering Plastic Gears," technical article, accessed January 2026. Available at: https://www.quandaplastic.com/how-to-choose-materials-for-engineering-plastic-gears/

[4] Beta Steel Group, "Common steel types/grades and common applications," Beta Steel blog, September 1, 2024, accessed January 2026. Available at: https://www.betasteel.com/blog/common-steel-typesgrades-and-common-applications_ae11.html

[5] SKF Group, "Bearing rating life," in Principles of rolling bearing selection, SKF online technical documentation, accessed January 2026. Available at: https://www.skf.com/mena/products/rolling-bearings/principles-of-rolling-bearing-selection/bearing-selection-process/bearing-size/size-selection-based-on-rating-life